Surrogate Modeling of Impedance Matching Transformers by Means of Variable-Fidelity EM Simulations and Nested Co-Kriging

Anna Pietrenko-Dabrowska[1] and Slawomir Koziel[2,1]

[1] Faculty of Electronics, Telecommunications and Informatics, Gdansk University of Technology, 80-233 Gdansk, Poland, anna.dabrowska@pg.edu.pl

[2] Engineering Optimization & Modeling Center, Reykjavik University, 101 Reykjavik, Iceland, koziel@ru.is,

Keywords: Microwave design; surrogate modeling; kriging interpolation; co-kriging; performance-driven modeling; EM-driven design.

Abstract

Accurate performance evaluation of microwave components can be carried out using full-wave electromagnetic (EM) simulation tools, routinely employed for circuit verification but also in the design process itself. Unfortunately, the computational cost of EM-driven design may be high. This is especially pertinent to tasks entailing considerable number of simulations (e.g., parametric optimization, statistical analysis). A possible way of alleviating these difficulties is utilization of fast replacement models, also referred to as surrogates. Notwithstanding, conventional modeling methods exhibit serious limitations when it comes to handling microwave components. The principal challenges include large number of geometry and material parameters, highly nonlinear characteristics, as well as the necessity of covering wide ranges of operating conditions. The latter is mandatory from the point of view of the surrogate model utility. This paper presents a novel modeling approach that incorporates variable-fidelity EM simulations into the recently reported nested kriging framework. A combination of domain confinement due to nested kriging, and low-/high-fidelity EM data blending through co-kriging, enables the construction of reliable surrogates at a fraction of cost required by single-fidelity nested kriging. Our technique is validated using a three-section miniaturized impedance matching transformer with its surrogate model rendered over wide range of operating frequencies. Comprehensive benchmarking demonstrates superiority of the proposed method over both conventional models and nested kriging.

1. Introduction

Contemporary microwave engineering heavily relies on full-wave electromagnetic (EM) simulation tools. Utilization of EM analysis is imperative in many situations, whenever simpler (analytical, equivalent network) models are unavailable or lack accuracy, e.g., due to the presence of strong cross-coupling effects [1]-[3]. Examples of such structures include compact components featuring tightly arranged layouts [4] or (Low Temperature Co-Firing) LTCC circuits [5]. One of the commonly executed EM-driven tasks is design closure [6], i.e., the adjustment of the system parameters, aimed at improving the performance figures of interest. Its major bottleneck is a high computational cost of the process, especially when large numbers of simulations are involved (e.g., global search [7], [8] or tolerance-aware design [9]).

Maintaining small size of components and devices (e.g., the fooprint area in the case of planar structures) is one of important design considerations of contemporary microwave engineering [10]-[14]. Miniaturized geometries, especially those implemented using slow-wave structures [15], [16] (e.g., compact microwave resonant cells, CMRCs [17], [18]) are often described by a large number of variables when compared to conventional transmission line (TL)-based circuit solutions. This incurs additional design challenges, in particular, an increased computational cost of parameter tuning [19], let alone the cost of design procedures involving massive simulations as mentioned previously. In some cases, the cost may be prohibitive when the design process is carried out directly at the level of full-wave simulations.

A reduction of the computational overhead of simulation-based design procedures is therefore a practical necessity. Extensive research conducted towards this end includes

the development of strictly algorithmic approaches (e.g., incorporation of adjoint sensitivities [20], sparse Jacobian updates [21], both in the context of gradient search methods) but also utilization of fast surrogate models. Surrogate-assisted methods are increasingly popular due to their potentially high efficacy in terms of providing means for rapid design in various aspects (parametric optimization [22], [23], statistical design [24], etc.). Some of the techniques developed over the last two decades or so include numerous types of space mapping (e.g., [25], [26]), response correction techniques [27], [28], or feature-based optimizers [29]. These methods are typically used for local search purposes. In terms of global search, efficient global optimization (EGO) frameworks [30], [31] are employed with the surrogate model iteratively constructed through sequential sampling [32]. The latter is often configured to both improve the model predictive power over the parameter space and seek for the global optimum.

An overall replacement of EM simulations by fast surrogate models (especially, the data-driven ones) is an attractive idea as it potentially enables low-cost execution of all sorts of simulation-based design procedures. Among many available modelling techniques, the following are particularly popular: polynomial regression [33], radial-basis functions [34], neural networks [35], [36], support-vector regression [37], kriging [38], and polynomial chaos expansion [39]. Notwithstanding, conventional techniques are rather limited in the sense of not being able to operate over highly-dimensional parameter spaces, handling nonlinear responses (common for many microwave components), and rendering models valid over wide ranges of geometry/material parameters and operating conditions. The latter is essential from the point of view of the model utility.

Mitigating some of the aforementioned issues is possible to a certain extent using methods such as high-dimensional model representation (HDMR) [40], orthogonal matching pursuit [41], or variable-fidelity frameworks (co-kriging [42], two-stage Gaussian Process Regression [43], Bayesian model fusion [44]). As indicated in [45], an appropriate selection of the surrogate model domain is another crucial aspect of the modelling process. In most cases, the lower and upper bounds for the system variables determine the region of interest. This leads to intractably large domains if the surrogate is to cover broad ranges of operating conditions. However, regardless of the particular choice of performance figures, high quality designs are normally allocated within small regions of the interval-type-of domains. This is because the optimum parameter sets are highly correlated. A representative example is dimension scaling with respect to the operating frequency, which requires (more or less) synchronized adjustment of many circuit parameters. From the point of view of the surrogate model construction, operating outside such "high quality" regions is a waste of resources. On the other hand, identification of the promising subset and focusing the modelling process therein may lead to substantial computational savings.

Recently, several methods exploiting this concept have been proposed in the literature, and referred to as constrained or performance-driven modelling [45]. In [46], focused on constrained modelling of microwave structures, the promising region of the parameter space was inferred from the pre-existing set of reference designs optimized for selected figures of interest. However, the number of performance figures in [46] was limited to one (the operating frequency); furthermore, the location of the reference designs was not arbitrary. The method of [47] lifted these restrictions. The primary

advantage of domain confinement is a dramatic reduction of its volume as compared to the original parameter space. This leads to a considerable reduction of the number of training data samples necessary to yield the surrogate. Unfortunately, the methods of [46] and [47] are characterized by complex geometries of the model domains, which limits their practical usefulness due to non-trivial implementation of design of experiments and model optimization. The recently proposed nested kriging framework [48] effectively addresses both issues through the establishment of a one-to-one mapping between the surrogate domain and a unity hypercube.

This work describes a novel development of low-cost and reliable surrogate modelling of microwave components by incorporating variable-fidelity EM simulations into the nested kriging of [48]. The overall objective is a further reduction of the CPU cost of surrogate model construction. This is achieved by operating within the confined domain of the nested kriging while blending densely sampled low-fidelity and sparsely sampled high-fidelity data using co-kriging [42]. The efficacy of the proposed procedure is demonstrated using a miniaturized impedance matching transformer. Comprehensive numerical studies indicate superiority of our method over both conventional data-driven surrogates (kriging, radial-basis functions) and the nested kriging involving high-fidelity data only. Supplementary application case studies (parametric optimization) confirm utility of the variable-fidelity surrogates rendered at the cost corresponding to less than two hundred high-fidelity simulations of the transformer structure.

2. Modeling Procedure

The purpose of this section is to briefly formulate the two fundamental components of the proposed modeling methodology, i.e., the nested kriging framework of [48], and co-kriging [42]. The role of the former is to establish the surrogate model domain, whereas the latter permits blending the low- and high-fidelity EM simulation data acquired within that domain. The section is concluded with the outline of the entire modeling flow. Section 3 presents demonstration examples and benchmarking.

2.1. Nested Kriging

The nested kriging modeling [48] is founded on the idea of constraining the surrogate model domain to a small region containing the designs that are of high-quality with respect to the set of performance figures pertinent to the structure at hand. This way, considerable computational savings can be achieved at the stage of training data acquisition: the volume of the aforementioned region is miniscule compared to that of the usual domain, here, denoted as X, and delimited by the lower bounds $\boldsymbol{l}$ and upper bounds $\boldsymbol{u}$ for the system variables.

The method of [48] constructs two kriging interpolation models. The first-level surrogate is employed to establish the domain. The second-level model is the actual surrogate. The figures of interest are denoted as f_k, $k = 1, \ldots, N$. These could be the target values of the operating frequencies, bandwidth, power split ratio, etc., but also material parameters (e.g., dielectric permittivity or height of the substrate the structure is implemented on). The objective space F is defined by the ranges $f_{k.\min} \leq f_k^{(j)} \leq f_{k.\max}$, $k = 1, \ldots, N$, to be covered by the surrogate.

The first-level surrogate $\boldsymbol{s}_I(\boldsymbol{f})$ is constructed to map F into the design space X. It is identified using the data set $\{\boldsymbol{f}^{(j)},\boldsymbol{x}^{(j)}\}$, $j = 1, \ldots, p$, as the training points, where $\boldsymbol{x}^{(j)} = [x_1^{(j)} \ldots x_n^{(j)}]^T$, are the reference designs optimized w.r.t. the performance vectors $\boldsymbol{f}^{(j)} = [f_1^{(j)} \ldots f_N^{(j)}]$, see also Fig. 1. These can be prepared beforehand, specifically for the purpose of surrogate model construction, or may be available from the prior design work concerning the same microwave structure.

The goal is to set up the surrogate model in the region $O(F) \subset X$ containing all designs that are optimum with respect to all $\boldsymbol{f} \in F$. The image $\boldsymbol{s}_I(F) \subset X$ of the objective space through the first-level surrogate provides an approximation of $O(F)$; however, its accuracy is limited because the number of reference designs is normally small (note that $\boldsymbol{x}^{(j)} \in O(F)$ for all $j = 1, \ldots, p$, because these designs are optimized for $\boldsymbol{f}^{(j)} \in F$). To ensure that the domain encapsulates the entire $O(F)$, $\boldsymbol{s}_I(F)$ needs to be enlarged. The nested kriging framework achieves this by an orthogonal extension of $\boldsymbol{s}_I(F)$ towards its normal vectors. Let us denote by $\{\boldsymbol{v}_n^{(k)}(\boldsymbol{f})\}$, $k = 1, \ldots, n - N$, an orthonormal basis of vectors normal to $\boldsymbol{s}_I(F)$ at the objective vector $\boldsymbol{f}$. Furthermore, we define $\boldsymbol{x}_{\max} = \max\{\boldsymbol{x}^{(k)}, k = 1, \ldots, p\}$, $\boldsymbol{x}_{\min} = \min\{\boldsymbol{x}^{(k)}, k = 1, \ldots, p\}$, and $\boldsymbol{x}_d = \boldsymbol{x}_{\max} - \boldsymbol{x}_{\min}$ as the parameter variations within $\boldsymbol{s}_I(F)$. Using these, the extension coefficients can be defined as

$$\boldsymbol{\alpha}(\boldsymbol{f}) = [\alpha_1(\boldsymbol{f}) \ldots \alpha_{n-N}(\boldsymbol{f})]^T = 0.5T\left[|\boldsymbol{x}_d \boldsymbol{v}_n^{(1)}(\boldsymbol{f})| \ \ldots \ |\boldsymbol{x}_d \boldsymbol{v}_n^{(n-N)}(\boldsymbol{f})|\right]^T \tag{1}$$

where T is a thickness parameter; α_k determine the bounds of the domain X_S, located between manifolds M_+ and M_- (cf. Fig. 1(b))

$$M_\pm = \left\{\boldsymbol{x} \in X : \boldsymbol{x} = \boldsymbol{s}_I(\boldsymbol{f}) \pm \sum_{k=1}^{n-N} \alpha_k(\boldsymbol{f}) \boldsymbol{v}_n^{(k)}(\boldsymbol{f})\right\} \tag{2}$$

The surrogate model domain X_S can be then defined as follows

$$X_S = \left\{ \begin{array}{c} \boldsymbol{x} = \boldsymbol{s}_1(\boldsymbol{f}) + \sum_{k=1}^{n-N} \lambda_k \alpha_k(\boldsymbol{f}) \boldsymbol{v}_n^{(k)}(\boldsymbol{f}) : \boldsymbol{f} \in F, \\ -1 \le \lambda_k \le 1, k = 1, ..., n-N \end{array} \right\} \quad (3)$$

The actual (second-level) kriging interpolation surrogate is established in X_S. The training data set is $\{\boldsymbol{x}_B^{(k)}, \boldsymbol{R}(\boldsymbol{x}_B^{(k)})\}_{k = 1, ..., NB}$, and it is acquired by allocating the points $\boldsymbol{x}_B^{(k)} \in X_S$ and evaluating the EM-simulation model $\boldsymbol{R}$ of the structure of interest. The design of experiments procedure as well as surrogate model optimization have been described in [48]. Again, the major advantage of setting up the surrogate within X_S rather than in X should be reiterated, which is a significantly smaller number of data samples required to render a reliable model without formally restricting the ranges of geometry parameters nor the ranges of the operating conditions.

2.2. Co-Kriging

The second component of the proposed modeling procedure is co-kriging briefly recalled in this section. Its purpose is to blend information from the low- and high-fidelity EM simulation models, thereby permit further reduction of the computational cost of the training data acquisition.

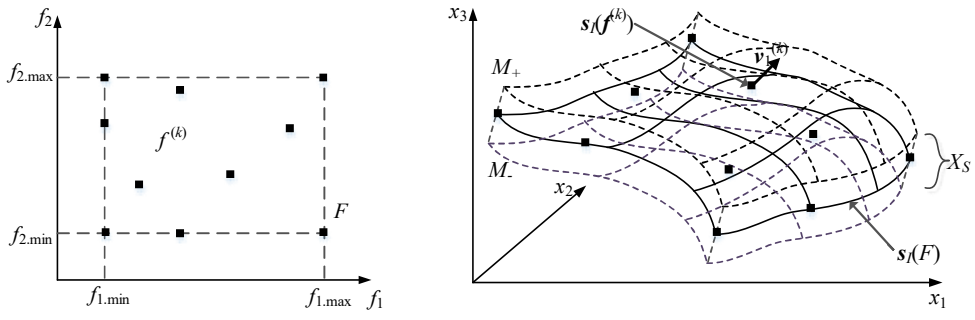

(a) (b)

Fig. 1. Nested kriging modeling [48]: (a) reference designs and the objective space F; (b) the image $\boldsymbol{s}_1(F)$ of the first-level surrogate and the normal vector $\boldsymbol{v}_1^{(k)}$ at $\boldsymbol{f}^{(k)}$; the manifolds M_- and M_+ as well as the surrogate model domain X_S defined as the orthogonal extension of $\boldsymbol{s}_1(F)$.

To begin with, we recall kriging interpolation. We denote by $X_{B.KR} = \{\boldsymbol{x}^1, \boldsymbol{x}^2, \ldots, \boldsymbol{x}^{NB}\}$ a set of training data samples and by $\boldsymbol{R}_f(X_{B.KR})$ the corresponding set of high-fidelity model responses. The kriging surrogate model $\boldsymbol{s}_{KR}(\boldsymbol{x})$ is defined as

$$\boldsymbol{s}_{KR}(\boldsymbol{x}) = M\gamma + r(\boldsymbol{x}) \cdot \Psi^{-1} \cdot (\boldsymbol{f}(X_{B.KR}) - \boldsymbol{F}\gamma) \tag{4}$$

in which M is a $N_B \times t$ model matrix of the training set $X_{B.KR}$ and $\boldsymbol{F}$ is a $1 \times t$ vector of the test node $\boldsymbol{x}$ and t is the number of terms used in the regression function [42]. The vector γ of the size $t \times 1$ stands for the regression function coefficients

$$\gamma = ({X_{B.KR}}^T \Psi^{-1} X_{B.KR})^{-1} X_{B.KR} \Psi^{-1} \boldsymbol{f}(X_{B.KR}) \tag{5}$$

whereas $r(\boldsymbol{x}) = (\psi(\boldsymbol{x}, \boldsymbol{x}_{KR}^1), ..., \psi(\boldsymbol{x}, \boldsymbol{x}_{KR}^{N_{KR}}))$ is an $1 \times N_B$ vector of correlations between the point $\boldsymbol{x}$ and the training set $X_{B.KR}$, and Ψ is a $N_B \times N_B$ correlation matrix where the entry of the i-th row and j-th column is given by $\Psi_{i,j} = \psi(\boldsymbol{x}_{KR}^i, \boldsymbol{x}_{KR}^j)$. The particular choice of the correlation function $\psi(\cdot,\cdot)$ plays an important role in creating a reliable kriging surrogate. A widely used class of correlation functions dependent only on the distance between any two points (here $\boldsymbol{x}$ and $\boldsymbol{x}'$) is defined by:

$$\psi(\boldsymbol{x}, \boldsymbol{x}') = \exp\left(\sum_{k=1}^{n} -\theta_k \mid x^k - x'^k \mid^p\right) \tag{6}$$

where n is the number of the design variables and the parameter p determines the prediction 'smoothness', whereas θ_k, $k = 1, \ldots, n$, are hyperparameters [42].

Usually, p is constant, whereas the hyperparameters are determined using Maximum Likelihood Estimation (MLE) [42], i.e., by solving

$$(\theta_1, ..., \theta_n) = \arg\min -(N_B / 2)\ln(\hat{\sigma}^2) - 0.5\ln(\mid \Psi \mid) \tag{7}$$

where

$$\hat{\sigma}^2 = (\boldsymbol{R}_f(X_{B.KR}) - F\alpha)^T \Psi^{-1} (\boldsymbol{R}_f(X_{B.KR}) - F\alpha) / N_B, \tag{8}$$

and $|\Psi|$ is the determinant of Ψ. Gaussian correlations functions corresponding to $p = 2$ are suitable for many practical problems. Assuming that no extrapolation capabilities are required, the regression function can be set constant, i.e., $\boldsymbol{F} = [1 \ \ldots \ 1]^T$ and $M = 1$.

Co-kriging can be considered an extension of kriging interpolation and it allows for combining information from the low- and high-fidelity computational models into a single surrogate. This is done by exploiting correlations between the models of various fidelities. Implementation-wise, two kriging models are sequentially produced [42]:

- Model $\boldsymbol{s}_{KRc}$ constructed using he low-fidelity data samples ($X_{B.KRc}$, $\boldsymbol{R}_c(X_{B.KRc})$), and
- Model $\boldsymbol{s}_{KRd}$ model generated on the residuals of the high- and low-fidelity samples ($X_{B.KRf}$, $\boldsymbol{r}$), where $\boldsymbol{r} = \boldsymbol{R}_f(X_{B.KRf}) - \rho\boldsymbol{R}_c(X_{B.KRf})$, where ρ is part of the MLE of the second model.

In case the low-fidelity model responses $\boldsymbol{R}_c(X_{B.KRf})$ are not available, they can be approximated using the first model as $\boldsymbol{R}_c(X_{B.KRf}) \approx \boldsymbol{s}_{KRc}(X_{B.KRf})$.

The particular configuration of the kriging models such as the correlation and regression functions can be decided upon independently for $\boldsymbol{s}_{KRc}$ and $\boldsymbol{s}_{KRd}$. Furthermore, both models use (6) as a correlation function together with constant regression function $\boldsymbol{F} = [1 \ 1 \ \ldots \ 1]^T$ and $M = 1$.

The ultimate co-kriging surrogate $\boldsymbol{s}_{CO}(\boldsymbol{x})$ is defined as

$$\boldsymbol{s}_{CO}(\boldsymbol{x}) = M\gamma + r(\boldsymbol{x}) \cdot \Psi^{-1} \cdot (\boldsymbol{r} - \boldsymbol{F}\gamma) \tag{9}$$

In (9), the block matrices M, $\boldsymbol{F}$, $r(\boldsymbol{x})$ and Ψ can be written as a function of the two kriging models $\boldsymbol{s}_{KRc}$ and $\boldsymbol{s}_{KRd}$:

$$r(\boldsymbol{x}) = [\rho \cdot \sigma_c^2 \cdot r_c(\boldsymbol{x}), \rho^2 \cdot \sigma_c^2 \cdot r_c(\boldsymbol{x}, X_{B.KR_f}) + \sigma_d^2 \cdot r_d(\boldsymbol{x})] \tag{10}$$

$$\Psi = \begin{bmatrix} \sigma_c^2 \Psi_c & \rho \cdot \sigma_c^2 \cdot \Psi_c(X_{B.KR_c}, X_{B.KR_f}) \\ 0 & \rho^2 \cdot \sigma_c^2 \cdot \Psi_c(X_{B.KR_f}, X_{B.KR_f}) + \sigma_d^2 \cdot \Psi_d \end{bmatrix} \tag{11}$$

$$F = \begin{bmatrix} F_c & 0 \\ \rho \cdot F_d & F_d \end{bmatrix}, \qquad M = [\rho \cdot M_c \;\; M_d] \tag{12}$$

in which (F_c, σ_c, Ψ_c, M_c) and (F_d, σ_d, Ψ_d, M_d) are the matrices obtained from $\boldsymbol{s}_{KRc}$ and $\boldsymbol{s}_{KRd}$, respectively; σ_c^2 and σ_d^2 are process variances, whereas $\Psi_c(\cdot,\cdot)$ and $\Psi_d(\cdot,\cdot)$ stand for the correlation matrices of two datasets with the optimized θ_k parameters and correlation function of $\boldsymbol{s}_{KRc}$ and $\boldsymbol{s}_{KRd}$, respectively.

2.3. Nested Co-Kriging: Modeling Procedure

Figure 2 shows the flow diagram of the modeling procedure. In the first stage, the model domain X_S is determined using the nested kriging of Section 2.1, whereas blending of low- and high-fidelity data samples is realized using co-kriging (cf. Section 2.2). In order to yield computational benefits, a larger number of the low-fidelity points supplements a small number of high-fidelity samples. The numerical experiments of Section 3 provide quantification of the effect of various proportions of the low-to-high-fidelity points on the surrogate model predictive power.

3. Verification Case Studies

This section discusses validation of the modeling procedure of Section 2. It is based on a compact microstrip impedance matching transformer described by fifteen geometry parameters. The numerical experiments presented below investigate various setups concerning the numbers of low- and high-fidelity samples utilized to construct the nested co-kriging surrogates, as well as benchmarking against conventional surrogates

(kriging and radial basis functions) and nested kriging based on high-fidelity simulation data only.

3.1. Case Study: Three-Section Miniaturized Impedance Matching Transformer

Consider a 50-to-100 ohm impedance matching transformer of Fig. 3. The circuit consists of three sections, all being CMRCs of Fig. 3(b). The structure is implemented on Taconic RF-35 substrate (ε_r = 3.5, h = 0.76). The design parameters are $\boldsymbol{x} = [l_{1.1}\ l_{1.2}\ w_{1.1}\ w_{1.2}\ w_{1.0}\ l_{2.1}\ l_{2.2}\ w_{2.1}\ w_{2.2}\ w_{2.0}\ l_{3.1}\ l_{3.2}\ w_{3.1}\ w_{3.2}\ w_{3.0}]^T$. The computational models are implemented in CST Microwave Studio. The high-fidelity model $\boldsymbol{R}_f$ contains around 300,000 mesh cells and simulated in around 150 seconds. The low-fidelity model $\boldsymbol{R}_c$ has ~100,000 cells with the simulation time of 60 seconds.

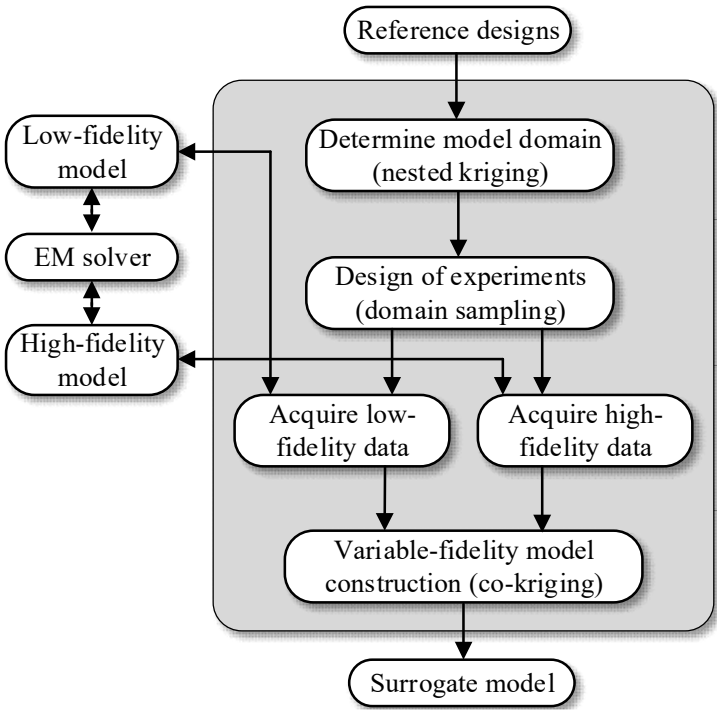

Fig. 2. Flowchart of variable-fidelity modeling using nested co-kriging.

(a) (b)

Fig. 3. CMRC-based impedance transformer: (a) topology of a three-section structure, (b) compact cell (CMRC).

3.2. Modeling Problem and Setup

The goal of the modeling process is construction of the surrogate that covers the operating bands [f_1 f_2] for 1.5 GHz $\leq f_1 \leq$ 3.5 GHz, and 4.5 GHz $\leq f_2 \leq$ 6.5 GHz. The first-level model is obtained using nine reference designs, optimized for all combinations of $f_1 \in$ {1.5, 2.5, 3.5} GHz and $f_2 \in$ {4.5, 5.5, 6.5} GHz. The lower and upper bounds for design variables, $\boldsymbol{l}$ = [2.0 0.15 0.65 0.35 0.30 2.70 0.15 0.44 0.15 0.30 3.2 0.15 0.30 0.15 0.30]^T, and $\boldsymbol{u}$ = [3.4 0.50 0.80 0.55 1.90 4.00 0.50 0.67 0.50 1.55 4.5 0.26 0.46 0.27 1.75]^T, are based on the reference points. It should be noted that modeling the three-section transformer is a challenging problem because of a large number of variables and wide ranges of the geometry parameters: the average ratio of the upper and lower bounds is around four.

Table 1 reports the numerical results obtained for various combinations of the high- and low-fidelity samples N_f and N_c, specifically: N_f = 20 and N_c = 400, N_f = 20 and N_c = 800, N_f = 50 and N_c = 400, as well as N_f = 50 and N_c = 800. The results are compared to conventional surrogates as well as the nested kriging model [48]. It can be observed that the model predictive power is slightly better than the nested kriging model obtained for 400 or 800 samples. Clearly, the benefit of using co-kriging is lower computational cost which is less around 200 equivalent high-fidelity evaluations for N_c = 400, and less than

400 equivalent high-fidelity evaluations for N_c = 800. Thus, the approach yields significant CPU savings despite the fact that the time evaluation ratio between $\boldsymbol{R_f}$ and $\boldsymbol{R_c}$ models is only 2.5. Figure 4 shows the transformer responses for the selected test designs, obtained for the model with 50 high-fidelity and 400 low-fidelity samples. A good visual alignment between the surrogate and the EM-simulated characteristics can be observed.

In order to demonstrate the nested co-kriging surrogate model utility, the circuit of Fig. 3(a) has been optimized for several operating bandwidths. Table 2 gathers the numerical results, whereas Figure 5 shows the transformer characteristics at the initial and the optimized designs. It can be observed that the initial design produced by the first-level surrogate is good in all considered design scenarios. At the same time, agreement between the surrogate and the EM simulated transformer response is reasonably good when evaluated at the surrogate-optimized design.

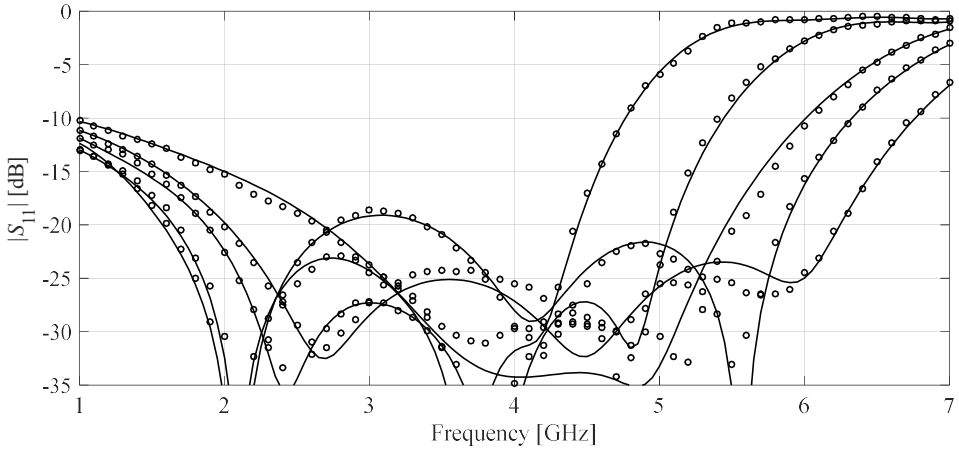

Fig. 4. Responses of the transformer of Fig. 3(a) at the selected test designs: EM model (—), nested co-kriging surrogate with N_f = 20 and N_c = 800 (o).

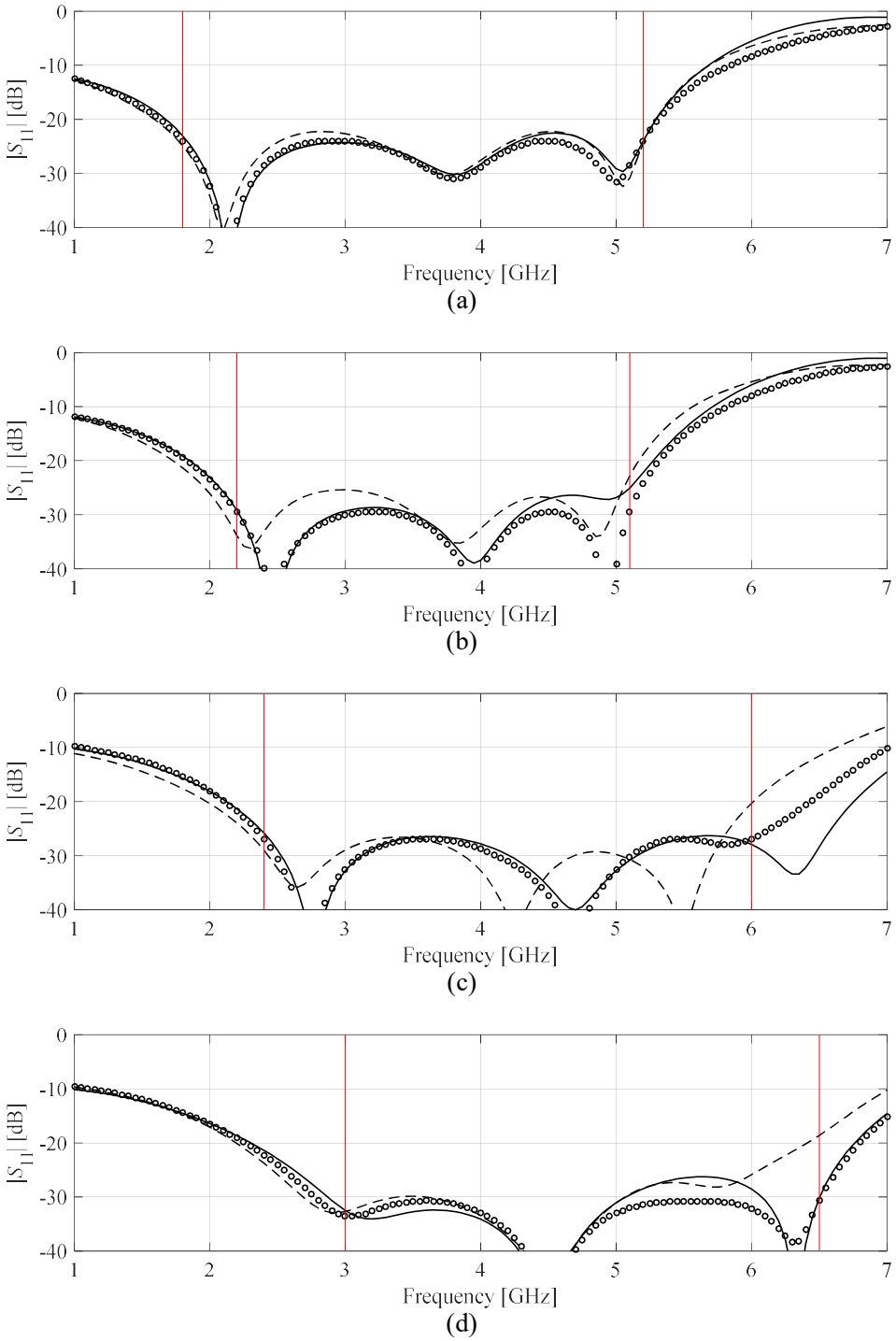

Fig. 5. Responses of the two-section transformer optimized with the nested co-kriging surrogate (generated for $N_f = 50$ and $N_c = 400$) for various target operating bands: (a) $f_1 = 1.8$ GHz, $f_2 = 5.2$ GHz, (b) $f_1 = 2.2$ GHz, $f_2 = 5.1$ GHz, (c) $f_1 = 2.4$ GHz, $f_2 = 6.0$ GHz, (d) $f_1 = 3.0$ GHz, $f_2 = 6.5$ GHz. Shown are: initial design (- - -), nested co-kriging surrogate (o), EM-simulated response at the optimized design (—).

Table 1. Modeling results for the three-section impedance transformer

Number of training samples	Relative RMS Error			Relative RMS Error			
	Conventional Models		Nested Kriging Model	Performance-driven modeling with nested co-kriging [this work]*			
	Kriging	RBF		$N_f = 20$ $N_c = 400$	$N_f = 20$ $N_c = 800$	$N_f = 50$ $N_c = 400$	$N_f = 50$ $N_c = 800$
50	49.1 %	56.2 %	17.3 %	6.8 % [180#]	5.4 % [340#]	5.7 % [210#]	4.9 % [370#]
100	31.1 %	33.0 %	13.9 %				
200	25.9 %	27.5 %	10.3 %				
400	20.4 %	23.1 %	7.4 %				
800	15.7 %	16.8 %	6.1 %				

* N_f and N_c stand for the number of high- and low-fidelity samples, respectively.
# The number is brackets is the total equivalent number of $\boldsymbol{R}_f$ samples used to set up the surrogate (calculated as $N_f + N_c/m$ where m is the time evaluation ratio between $\boldsymbol{R}_f$ and $\boldsymbol{R}_c$).

Table 2. Optimization results for the three-section impedance transformer

Target operating band		Geometry parameter values [mm]														
f_1 [GHz]	f_2 [GHz]	$l_{1.1}$	$l_{1.2}$	$w_{1.1}$	$w_{1.2}$	$w_{1.0}$	$l_{2.1}$	$l_{2.2}$	$w_{2.1}$	$w_{2.2}$	$w_{2.0}$	$l_{3.1}$	$l_{3.2}$	$w_{3.1}$	$w_{3.2}$	$w_{3.0}$
1.8	5.2	3.13	0.19	0.77	0.44	0.68	3.76	0.25	0.56	0.20	0.46	4.05	0.16	0.34	0.17	1.24
2.2	5.1	2.90	0.22	0.78	0.52	0.95	3.78	0.23	0.58	0.22	0.64	4.00	0.16	0.34	0.17	1.00
2.4	6.0	2.16	0.31	0.77	0.46	0.93	3.23	0.16	0.68	0.14	0.50	3.37	0.16	0.38	0.15	0.33
3.0	6.5	2.23	0.32	0.79	0.51	0.97	3.21	0.16	0.66	0.14	0.55	3.35	0.15	0.36	0.15	0.34

4. Conclusion

The paper introduced a methodology for low-cost and reliable surrogate modeling of miniaturized microwave components. The two keystones of the approach are the nested kriging modeling framework and the employment of variable-fidelity electromagnetic simulations, incorporated into the surrogate by means of co-kriging. Consequently, our methodology combines the benefits that arise from confining the domain of the surrogate with further computational savings coming due to acquisition of

most of the training data samples at the low-fidelity simulation level. The presented technique has been thoroughly validated using a miniaturized impedance matching transformer described by fifteen geometry parameters. The obtained results demonstrate that accurate models can be constructed over wide ranges of operating conditions using small training data sets. The predictive power of the nested co-kriging surrogates is comparable or better than that of the nested kriging using single-fidelity simulations yet achieved at a fraction of the CPU cost required by the latter. At the same time, the practical utility of our approach has been validated through application case studies (transformer optimization). The presented modeling technique may be useful for handling problems featuring highly-dimensional parameter spaces and nonlinear characteristics, especially when the surrogate is to be valid over broad ranges of the system parameters and operating conditions, i.e., the cases which are beyond the reach of conventional methods.

Acknowledgement

The authors would like to thank Dassault Systemes, France, for making CST Microwave Studio available. This work is partially supported by the Icelandic Centre for Research (RANNIS) Grant 174114051 and by National Science Centre of Poland Grant 2018/31/B/ST7/02369.

References

[1] J. Acharjee, K. Mandal, and S.K. Mandal, "Reduction of mutual coupling and cross-polarization of a MIMO/diversity antenna using a string of H-shaped DGS," *AEU – Int. J. Electr. Comm.*, vol. 97, pp. 110-119, 2018.

[2] H. Zhu and A.M. Abbosh, "A compact tunable directional coupler with continuously tuned differential phase," *IEEE Microwave Wireless Comp. Lett.*, vol. 28, no. 1, pp. 19-21, 2017.

[3] S. Liu and F. Xu, "Compact multilayer half mode substrate integrated waveguide 3-dB coupler," *IEEE Microwave Wireless Comp. Lett.*, vol. 28, no. 7, pp. 564-566, 2018.

[4] J. Elking, E. Goldberger, and E. Socher, "57-67-GHz highly compact bidirectional 3-bit phase shifter in 28-nm CMOS," *IEEE Microwave Wireless Comp. Lett.*, vol. 28, no. 11, pp. 1017-1019, 2018.

[5] W. Feng, X. Gao, W. Che, W. Yang, and Q. Xue, "LTCC wideband bandpass filters with high performance using coupled lines with open/shorted stubs," *IEEE Trans. Comp. Packaging Manufacturing Techn.*, vol. 7, no. 4, pp. 602-609 , 2017.

[6] X. Gao, H. M. Lee, and S. Gao, "A robust parameter design of wide band DGS filter for common-mode noise mitigation in high-speed electronics," *IEEE Trans. Electr. Comp.*, vol. 59, no. 6, pp. 1735-1740, 2017.

[7] B. Liu, H. Yang and M.J. Lancaster, "Global optimization of microwave filters based on a surrogate model-assisted evolutionary algorithm," *IEEE Trans. Microwave Theory Tech.*, vol. 65, no. 6, pp. 1976-1985, 2017.

[8] M.C. Tang, X. Chen, M. Li, and R.W. Ziolkowski, "Particle swarm optimized, 3-D-printed, wideband, compact hemispherical antenna," *IEEE Ant. Wireless Prop. Lett.*, vol. 17, no. 11, pp. 2031-2035, 2018.

[9] A.S. Abd El-Hameed, M.G. Wahab, A. Elboushi, and M.S. Elpeltagy, "Miniaturized triple band-notched quasi self-complementary fractal antenna with improved characteristics for UWB applications," *AEU – Int. J. Electr. Comm.*, vol. 108, pp. 163-171, 2019.

[10] S. Koziel and P. Kurgan, "Selection of circuit geometry for miniaturized microwave components based on concurrent optimization of performance and layout area, *AEU – Int. J. Electr. Comm.*, vol. 109, pp. 287-294, 2019.

[11] S. Koziel and J.W. Bandler, "Rapid yield estimation and optimization of microwave structures exploiting feature-based statistical analysis," *IEEE Trans. Microwave Theory Tech.*, vol. 63, no., 1, pp. 107-114, 2015.

[12] L. Martinez, A. Belenguer, V.E. Boria, and A.L. Borja, "Compact folded bandpass filter in empty substrate integrated coaxial line at S-band," *IEEE Microwave Wireless Comp. Lett.*, vol. 29, no. 5, pp. 315-317, 2019.

[13] A. Contreras, M. Ribo, L. Pradell, V. Raynal, I. Moreno, M. Combes, and M. Ten, "Compact fully uniplanar bandstop filter based on slow-wave multimodal CPW resonators," *IEEE Microwave Wireless Comp. Lett.*, vol. 28, no. 9, pp. 780-782, 2018.

[14] H. Tian, K.L. Chung, R. Liu, M. Dai, and W. Tang, "Miniaturized quadrature hybrid coupler using composite planar transmission lines," *El. Lett.*, vol. 55, no. 19, pp. 1049-1051, 2019.

[15] C.H. Tseng and C.L. Chang, "A rigorous design methodology for compact planar branch-line and rat-race couplers with asymmetrical T-structures," *IEEE Trans. Microw. Theory Techn.*, vol. 60, no. 7, pp. 2085–2092, 2012.

[16] A. Parameswaran and S. Raghavan, "Pseudo-elliptic slow wave line," *AEU – Int. J. Electr. Comm.*, vol. 97, pp. 130-136, 2018.

[17] S. Koziel and P. Kurgan, "Compact cell topology selection for size-reduction-oriented design of microstrip rat-race couplers," *Int. J. RF & Microwave CAE*, vol. 28, no. 5, 2018.

[18] L. Huang, W. Wu, X. Zhang, H. Lu, Y. Zhou, and N. Yuan," A novel compact and high performance bandpass filter based on SIW and CMRC technique*, AEU – Int. J. Electr. Comm.*, vol. 82, pp. 420-425, 2017.

[19] P. Kurgan, and S. Koziel, "Fast surrogate-assisted simulation-driven design of compact microwave hybrid couplers," *Eng. Optimization*, vol. 48, no. 7, pp. 1109-1120, 2016.

[20] H. Malhi and M.H. Bakr, "Geometry evolution of microwave filters exploiting self-adjoint sensitivity analysis," *Int. Conf. Numerical Electromagnetics and Multiphysics Mod. Opt. (NEMO)*, Ottawa, Canada, 11-14 Aug. 2015.

[21] A. Pietrenko-Dabrowska and S. Koziel, "Numerically efficient algorithm for compact microwave device optimization with flexible sensitivity updating scheme," *Int. J. RF & Microwave CAE*, vol. 29, no. 7, 2019.

[22] J. Dong, Q. Li, and L. Deng, "Fast multi-objective optimization of multi-parameter antenna structures based on improved MOEA/D with surrogate-assisted model", *AEU – Int. J. Electr. Comm.*, vol. 72, pp. 192-199, 2017.

[23] J. Dong, W. Qin, and M. Wang, "Fast multi-objective optimization of multi-parameter antenna structures based on improved BPNN surrogate model," *IEEE Access*, vol. 7, pp. 77692-77701, 2019.

[24] J. Zhang, C. Zhang, F. Feng, W. Zhang, J. Ma and Q.J. Zhang, "Polynomial chaos-based approach to yield-driven EM optimization," *IEEE Trans. Microwave Theory Tech.*, vol. 66, no. 7, pp. 3186-3199, 2018.

[25] C. Zhang, F. Feng, Q. Zhang and J.W. Bandler, "Enhanced cognition-driven formulation of space mapping for equal-ripple optimisation of microwave filters," *IET Microwaves Ant. Prop.*, vol. 12, no. 1, pp. 82-91, 2018.

[26] I.A. Baratta, C.B. de Andrade, R.R. de Assis, and E.J. Silva, "Infinitesimal dipole model using space mapping optimization for antenna placement," *IEEE Ant. Wireless Prop. Lett.*, vol. 17, no. 1, pp. 17-20, 2018.

[27] Y. Su, J. Li, Z. Fan, and R. Chen, "Shaping optimization of double reflector antenna based on manifold mapping," *Int. Applied Comp. Electromagnetic Society Symp. (ACES)*, Suzhou, China, 1-4 Aug. 2017.

[28] S. Koziel and S.D. Unnsteinsson "Expedited design closure of antennas by means of trust-region-based adaptive response scaling," *IEEE Antennas Wireless Prop. Lett.*, vol. 17, no. 6, pp. 1099-1103, 2018.

[29] S. Koziel, "Fast simulation-driven antenna design using response-feature surrogates," *Int. J. RF & Micr. CAE*, vol. 25, no. 5, pp. 394-402, 2015.

[30] Y. Li, S. Xiao, M. Rotaru, and J.K. Sykulski, "A dual kriging approach with improved points selection algorithm for memory efficient surrogate optimization in

electromagnetics," *IEEE Trans. Magnetics*, vol. 52, no. 3, paper No. 7000504, 2016.

[31] G. Sun, Y. Liu, S. Liang, A. Wang, Y. Zhang," Beam pattern design of circular antenna array via efficient biogeography-based optimization," *AEU – Int. J. Electr. Comm.*, vol. 79, pp. 275-285, 2017.

[32] H.M. Torun and M. Swaminathan, "High-dimensional global optimization method for high-frequency electronic design," *IEEE Trans. Microwave Theory Techn.*, vol. 67, no. 6, pp. 2128-2142, 2019.

[33] J.L. Chavez-Hurtado and J.E. Rayas-Sanchez, "Polynomial-based surrogate modeling of RF and microwave circuits in frequency domain exploiting the multinomial theorem," *IEEE Trans. Microwave Theory Tech.*, vol. 64, no. 12, pp. 4371-4381, 2016.

[34] P. Barmuta, F. Ferranti, G.P. Gibiino, A. Lewandowski and D.M.M.P. Schreurs, "Compact behavioral models of nonlinear active devices using response surface methodology," *IEEE Trans. Microwave Theory Tech.*, vol. 63, no. 1, pp. 56-64, 2015.

[35] W. Liu, W. Na, L. Zhu, J. Ma and Q.J. Zhang, "A Wiener-type dynamic neural network approach to the modeling of nonlinear microwave devices," *IEEE Trans. Microwave Theory Tech.*, vol. 65, no. 6, pp. 2043-2062, 2017.

[36] A. Kayabasi, "Soft computing-based synthesis model for equilateral triangular ring printed antenna," *AEU – Int. J. Electr. Comm.*, vol. 94, pp. 332-338, 2018.

[37] J. Cai, J. King, C. Yu, J. Liu and L. Sun, "Support vector regression-based behavioral modeling technique for RF power transistors," *IEEE Microwave and Wireless Comp. Lett.*, vol. 28, no. 5, pp. 428-430, 2018.

[38] D.I.L. de Villiers, I. Couckuyt and T. Dhaene, "Multi-objective optimization of reflector antennas using kriging and probability of improvement," *Int. Symp. Ant. Prop.*, pp. 985-986, San Diego, USA, 2017.

[39] A.K. Prasad and S. Roy, "Accurate reduced dimensional polynomial chaos for efficient uncertainty quantification of microwave/RF networks," *IEEE Trans. Microwave Theory Tech.*, vol. 65, no. 10, pp. 3697-3708, 2017.

[40] H. Liu, J.R. Hervas, Y.S. Ong, J. Cai, and Y. Wang, "An adaptive RBF-HDMR modeling approach under limited computational budget," *Struct. Multidisc. Optim.*, vol. 57, no. 3, pp. 1-18, 2018.

[41] J.A. Tropp and A.C. Gilbert, "Signal recovery from random measurements via orthogonal matching pursuit," *IEEE Trans. Inf. Theory*, vol. 53, no. 12, pp. 4655-4666, 2007.

[42] M.C. Kennedy and A. O'Hagan, "Predicting the output from complex computer code when fast approximations are available", *Biometrika*, vol. 87, pp. 1-13, 2000.

[43] J.P. Jacobs and S. Koziel, "Two-stage framework for efficient Gaussian process modeling of antenna input characteristics," *IEEE Trans. Antennas Prop.*, vol. 62, no. 2, pp. 706-713, 2014.

[44] F. Wang, P. Cachecho, W. Zhang, S. Sun, X. Li, R. Kanj and C. Gu, "Bayesian model fusion: large-scale performance modeling of analog and mixed-signal

circuits by reusing early-stage data," *IEEE Trans. on Computer-Aided Design of Integrated Circuits and Systems (TCAD)*, vol. 35, no. 8, pp. 1255-1268, 2016.

[45] S. Koziel, "Low-cost data-driven surrogate modeling of antenna structures by constrained sampling," *IEEE Antennas Wireless Prop. Lett.*, vol. 16, pp. 461-464, 2017.

[46] S. Koziel and A. Bekasiewicz, "Accurate design-oriented simulation-driven modeling of miniaturized microwave structures," *Int. J. Numerical Modelling*, vol. 29, no. 6, pp. 1028-1035, 2016.

[47] S. Koziel and A.T. Sigurðsson, "Performance-driven modeling of compact couplers in restricted domains," *Int. J. of RF and Microwave CAE*, vol. 28, no. 6, 2018.

[48] S. Koziel and A. Pietrenko-Dabrowska, "Performance-based nested surrogate modeling of antenna input characteristics," *IEEE Trans. Ant. Prop.*, vol. 67, no. 5, pp. 2904-2912, 2019.